International Journal of Hydrogen Energy 59 (2024) 755–763

Contents lists available at ScienceDirect

International Journal of Hydrogen Energy

journal homepage: www.elsevier.com/locate/he

Catalytically driven hydrogen storage in magnesium hydride through its chemical interaction with the additive vanadium pentoxide

D. Pukazhselvan [a,b,*], Ihsan Çaha [c], Laura IV Holz [a,b], Francis Leonard Deepak [c], Peter Kjær Kristensen [d], Riccardo Checchetto [e], Frede Blaabjerg [f], Duncan Paul Fagg [a,b]

[a] TEMA - Centre for Mechanical Technology and Automation, Department of Mechanical Engineering, University of Aveiro, 3810-193, Aveiro, Portugal
[b] LASI - Intelligent Systems Associate Laboratory, 4800-058, Guimarães, Portugal
[c] Nanostructured Materials Group, International Iberian Nanotechnology Laboratory (INL), Avenida Mestre Jose Veiga, Braga, 4715-330, Portugal
[d] Department of Materials and Production Aalborg University, Skjernvej 4A, DK-9220, Aalborg East, Denmark
[e] Department of Physics, University of Trento, Via Sommarive, 14, 38123, Povo, Italy
[f] Department of Energy Technology, Aalborg University, Pontoppidanstræde 101, 76, 9220, Aalborg, Denmark

ARTICLE INFO

Handling Editor: Ibrahim Dincer

Keywords:
Hydrogen storage
Metal oxides
Reaction kinetics
Reaction mechanism

ABSTRACT

Considering the importance of understanding the catalysis of metal oxides incorporated hydrogen storage system MgH_2, in this study we tried to identify the chemical interaction between magnesium hydride (MgH_2) and the additive vanadium pentoxide (V_2O_5). Two test samples, MgH_2+0.25V_2O_5 and 0.25MgH_2+V_2O_5, were subjected to mechanical milling treatment for different times (15 min, 1h, 2h, 5h, 10h and 15h), and the phase change was monitored systematically. The detailed X ray diffraction analyses suggest that the phase evolution starts with the reduction of V_2O_5 and it ends up with the formation of a rock salt structure, typified by $Mg_xV_yO_{x+y}$. High-resolution transmission electron microscopy study coupled with energy dispersive spectroscopy suggest that the distribution of V, Mg and O in $Mg_xV_yO_{x+y}$ is homogenous, though V-rich spots/boundaries can be spotted across the rock salt particles. Further verification by X–ray photoelectron spectroscopy suggests that V exists in a mixed valence state in the end sample, 15h reacted MgH_2+0.25V_2O_5. Differential scanning calorimetry and hydrogen storage kinetics studies prove the improved hydrogen storage behavior of $Mg_xV_yO_{x+y}$ containing MgH_2 sample. We believe that the formation of $Mg_xV_yO_{x+y}$ rock salt particles with V enriched spots/interfaces is the key step in the catalysis of V_2O_5 incorporated hydrogen storage system, MgH_2.

1. Introduction

The development of a compact hydrogen fuel tank with the ability to reversibly deliver 5.5 wt% hydrogen at a maximum operating temperature of 85 °C is crucial for the successful demonstration of hydrogen fuel cell vehicles [1,2]. In this context, among the several reversible solid-state hydrogen storage materials studied globally, magnesium hydride is considered promising, mainly due to its high theoretical capacity (gravimetric capacity: 7.6 wt% H_2, volumetric capacity: 110 g H_2/L). However, few issues such as, poor dehydrogenation kinetics and high operational temperature (>350 °C) remain the limitations of pure MgH_2 samples, and identifying a solution to these issues is necessary for making MgH_2 a potentially useful material for vehicular applications [3]. Recent studies suggest that MgH_2 can be kinetically improved by incorporating suitable additives and it is possible to lower the operational temperature by at least 50–100 °C [4–12]. Especially, metal oxides are the widely studied additives among the several classes of transition metal compounds reported in the literature [13–20]. It is revealed that the metal oxides improve the hydrogen storage behavior of MgH_2 by making active in situ catalytic species through chemical interaction with MgH_2 [21–23]. For the past few years, the current team has been investigating how metal oxides interact with MgH_2 and generate active catalytic species. We have reported detailed studies on TiO_2 [24,25], Nb_2O_5 [26,27], CeO_2 [28,29], ZrO_2 [30,31] and other mixed/ternary oxides [14,32] as additives and the underlying chemical phenomenon for exploring the hydrogen storage mechanism of MgH_2. In this context, in the current work our aim is to investigate how yet another metal oxide V_2O_5 produces active catalytic species through its

* Corresponding author. TEMA - Centre for Mechanical Technology and Automation, Department of Mechanical Engineering, University of Aveiro, 3810-193, Aveiro, Portugal.
E-mail addresses: dpuksel@gmail.com, dpukazh@ua.pt (D. Pukazhselvan).

https://doi.org/10.1016/j.ijhydene.2024.02.037
Received 29 November 2023; Received in revised form 12 January 2024; Accepted 3 February 2024

interaction with MgH_2. Understanding how this interaction compares or contrasts with the previously studied oxides can provide great insights for the formulation of a generalized catalytic mechanism of metal oxide systems. In fact V_2O_5 and its derivatives were previously investigated by a few researchers and all these investigations agree that V_2O_5 is a promising additive for MgH_2. However, as far as the discussion on the catalytic mechanism is concerned, considerable anomalies can be noted mainly because different opinions were derived regarding the chemical identity of the active species.

Dai et al. [33] observed that a 5 wt% V_2O_5 added MgH_2 absorbs 3.8 wt%.H_2 at a 30-bar hydrogen pressure under room temperature and this capacity can be increased to 6.7 wt% when the temperature is raised to 300 °C. Through XPS investigation the authors observed that the dehydrogenated sample contains vanadium species with V^{3+} state and the chemical state remains unchanged after restoring hydrogen. Wang et al. [34] synthesized carbon supported V_2O_3 from a metal organic framework MIL 47(V) and found that a 9 wt% V_2O_3@C added MgH_2 releases 6.4 wt% H_2 at 275 °C and all the released hydrogen can be restored within 20 s when hydrogenated with a pressure of 50 bars at 150 °C. They have also observed that the milled powder contains MgO and reduced vanadium, and the catalytic activity was therefore attributed to the presence of reduced vanadium nanoparticles. Oelerich et al. [35] have tested several metal oxide nanoparticles such as, Sc_2O_3, TiO_2, V_2O_5, Cr_2O_3, Mn_2O_3, Fe_3O_4, CuO, Al_2O_3, SiO_2 as additives for MgH_2 and found that a mere 1 mol.% concentration of V_2O_5 performs better than all other additives. For instance, 6.5 wt% hydrogen release at 300 °C under vacuum can be achieved within 5 min, which is 6 times better kinetics as compared to the MgH_2 nanoparticles processed under identical conditions. Oelerich et al. have further made a comparative study [36] between a 5 mol.% of V, V_2O_5, VN, and VC as additives for MgH_2 and found that V_2O_5 is the best additive and, especially ultra-pure V nanoparticles present no observable catalytic effect. Korablov et al. [16] used TiH_2, ZrH_2, VCl_3, $ScCl_3$ and V_2O_5 as additives for MgH_2 and found that V_2O_5 is the best additive as compared to all these additives for fast hydrogen absorption/desorption interactions under identical testing conditions. The synchrotron XRD experiments performed in this study provides clear evidence for the existence of MgO in considerable quantities along with the traces of V and V_2H. With these observations, the authors suggested an interfacial effect between MgO/Mg/MgH_2/V as a probable factor for the improved system performance. Grigorova et al. [37] tested a composite powder, 90 wt% MgH_2 + 10 wt% V_2O_5 prepared by mechanical milling technique and observed that 6.3 wt% hydrogen can be reversibly stored under the testing conditions of 350 °C/1.5 bar (dehydrogenation) and 300 °C/10 bar (hydrogenation). The authors highlighted that Mg–V–O phases may be responsible for the improved system performance. One can observe in the literature that Mg–V–O phases were previously studied (Carrazán et al.) for the catalytic dehydrogenation of hydrocarbons and excellent results were observed [38,39]. Jung et al. [40] performed a comparative study between V_2O_5, Cr_2O_3, Al_2O_3 and Fe_2O_3 as additives (5 mol.%) for MgH_2 and found that V_2O_5 is the best additive for faster kinetics at low temperatures (200–250 °C). In this study, the authors suggested that the defects introduced through mechanical milling may be the reason for the improved system performance. One would clearly note from all these interesting studies that the opinions on catalysis remain considerably different between researchers, and hence this chapter requires rigorous further studies.

Keeping the above in view, in the interest of exploring the catalysis of V_2O_5 added MgH_2, in the current study we demonstrate the mechanochemical interaction of MgH_2/V_2O_5 composite powder samples. After initially studying two samples (MgH_2+0.25V_2O_5 and 0.25MgH_2+V_2O_5) by X - ray diffraction technique, an informative sample (MgH_2+0.25V_2O_5) is further studied by transmission electron microscopy and X ray photoelectron spectroscopy techniques. Subsequently, hydrogen storage measurements were performed and the important aspects correlating with the characterization results were identified. Moreover, by referring our previous studies on TiO_2 and Nb_2O_5 additives incorporated MgH_2 [24–27], a few interesting highlights are provided regarding the formulation of a generalized catalytic mechanism of oxides incorporated MgH_2 system for hydrogen storage applications.

2. Experimental

Vanadium pentoxide (V_2O_5) used in the current study was procured from Merck Chemicals Inc. Magnesium hydride used in the current study was synthesized in our laboratory from the commercially procured Mg granules (Nanografi). For the synthesis of MgH_2 the following three steps were followed, (i) ball milling of the coarse Mg particles at the speed of 350 rpm for 20h under inert atmosphere, (ii) hydrogenation of the ball milled sample in pure hydrogen atmosphere under 70 bar at 370 °C, (iii) ball milling the observed product again for 5h and repeating the hydrogenation at 70 bar at 370 °C for 5h. This procedure led to the formation of pure MgH_2 particles. After the synthesis of fresh MgH_2 samples, MgH_2 and V_2O_5 were mixed in 4:1 and 1:4 M ratios and ball milled at the speed of 350 rpm with different time intervals (details in the results section). All the ball milling operations in the current study were performed by using a planetary ball milling facility, Retsch PM200, where the milling medium is stainless steel with a ball to powder weight ratio of 70:1 (For useful information regarding a comparison between stainless steel and zirconia milling medium on the quality of the derived powder samples (MgH_2 based samples), we recommend the reader to refer our previous study [41]). Two additives were used in the current study for MgH_2, (i) as-received V_2O_5, (ii) product observed after ball milling MgH_2+0.25V_2O_5 for 15h. For convenience these additives were assigned with the codes A1 and A2. Powder processing was performed inside an Ar filled MBraun glove box.

Freshly prepared samples were initially characterized by the X-ray diffraction technique. The XRD specimen holder was sealed inside the glove box by polyimide films to prevent air/moisture induced contamination effects during the XRD measurements. A Rigaku X-ray diffractometer with a CuKα radiation source (wavelength, 1.541 Å) was employed. Information regarding the lattice structure in samples A1 and A2 was obtained through the XRD patterns using Rietveld refinement technique [42] as implemented in the SmartLab Studio package. We used pseudo-Voigt peak profile function for profile fitting and B-spline function for background fitting. Transmission Electron Microscopy (TEM), Scanning Transmission Electron Microscopy (STEM) and energy-dispersive X-ray spectroscopy (EDX) studies were performed by using a double corrected FEI Titan G3 Cubed Themis equipped with a Super-X EDX System, operating at 200 kV. For these studies, fresh samples were prepared by firstly dispersing the powder in ethanol and then drop-casting this on a holey carbon Cu grid under inert processing conditions. The grids were vacuum dried at 35 °C for 30 min before measurement. Differential scanning calorimetry (DSC) measurements were performed by a DSC 5000 PERKIN ELMER thermal analyzer facility. The measurement is calibrated with a Cu reference where N_2 is a carrier gas with the flow rate of 20 cc/minute. The hydrogen storage measurements were performed by using a Sieverts volumetric measurement facility developed in our laboratory. Before measurements the samples were evacuated, and dehydrogenation was performed under pure hydrogen atmosphere at the pressure of 1 bar at 300 °C. Subsequent hydrogenation was performed at the same temperature at 5 bar hydrogen pressure. X - ray photoelectron spectroscopy measurements were done with a Specs XR50 non-monochromated X-ray source using the Al Kα line from an Al cathode running at 300W, and the photoelectrons were detected using Specs Phoibos 150 1D-DLD. The powder was lodged on a piece of silicon wafer using double-sided carbon tape.

3. Results and discussion

In our previous study we tested TiO_2 as an additive for MgH_2 and found that the powder contains catalytically active new in-situ product,

typified by $Mg_xTi_yO_{x+y}$. By investigating a composite MgH_2+0.5TiO_2 we found that the formation of $Mg_xTi_yO_{x+y}$ can be explored in good detail and it provides understanding regarding how TiO_2 added MgH_2 system works at lower temperatures [25]. Hence, by treating this as a reference case, for the current study we prepared a composite MgH_2 + 0.25V_2O_5 as the Mg to V atomic ratio (2:1) used in the current case is comparable to the Mg:Ti ratio used in the previous study.

The additives used in the current study are assigned the codes, A1 and A2. The additive A1 is the as-received V_2O_5, whereas A2 is the mechanochemically activated composite powder, MgH_2 + 0.25V_2O_5 (more info in the experimental section). In Fig. 1, we provide the observed XRD pattern corresponding to the additives A1 and A2. In the case of A2, the XRD shows no traces of MgH_2/V_2O_5 and it is clear that the ingredients interacted chemically upon mechanical milling. With further analysis it is found that the observed set of peaks in A2 correspond to MgO type rock salt structure (for reference, XRD of a standard MgO rock salt powder is also provided in the figure). For more clarity, the structural details of the observed phase in A2 were identified through the Rietveld refinement method and the details are summarized in Table 1. The main phase in A2 correspond to a periclase type MgO rock salt with space group 225:Fm-3m and cubic lattice structure with lattice parameters, a = b = c = 4.2146 Å (for further details, such as crystallite size, cell volume and strain percentage, refer to Table 1). For reference we have also calculated the structural parameters of the standard MgO rock salt sample and summarized this in Table 1. The dominant presence of MgO in A2 suggests that V_2O_5 is chemically reduced by interacting with MgH_2 but it is surprising that no traces of V in any XRD discernible phases can be explored. This is in similarity with the previously studied systems Nb_2O_5/MgH_2 and TiO_2/MgH_2 where it was proven that the absence of Nb/Ti as a separate phase is because Mg/Ti dissolved in the MgO rock salt (typified by $Mg_xTi_yO_{x+y}$/$Mg_xNb_yO_{x+y}$) [24–27,32,41]. A similar situation may occur in the current case also, hence in the following sections, we analyzed in detail (i) the systematic transformation of MgH_2+0.25V_2O_5 mixture as a mono-phase rock salt oxide (the end product of A2), (ii) the influence of the end product A2 on the dehydrogenation behavior of MgH_2. We believe that such a detailed investigation would provide a thorough insight regarding how MgH_2 and the additive V_2O_5 chemically interact and subsequently catalyze the remaining MgH_2. Pictures regarding how these transformation compares or contrasts with the results known for the other studied oxides (for e.g. Nb_2O_5/TiO_2, etc.) will provide clues for formulating a generalized catalytic mechanism for metal oxides incorporated MgH_2 system for hydrogen storage applications.

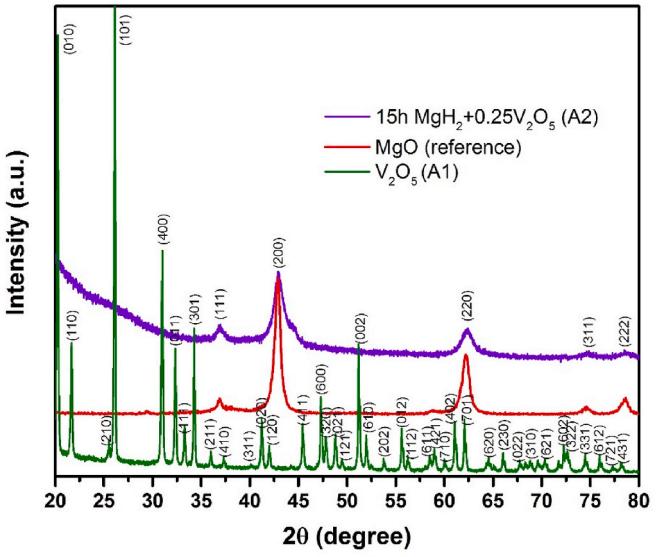

Fig. 1. XRD patterns correspond to the additives A1 (V_2O_5) and A2 (15h reacted MgH_2+0.25V_2O_5) used in the current study. The standard XRD pattern corresponding to clean MgO is provided for comparison.

To understand how MgH_2+0.25V_2O_5 gradually transforms as a single-phase rock salt oxide, the reaction time of the mixture MgH_2+0.25V_2O_5 was varied from an initial shorter time of 15 min, and then in different time intervals the product was monitored. Fig. 2 shows the XRD patterns observed for the MgH_2 + 0.25V_2O_5 sample ball milled for 15 min, 1h, 2h, 5h, 10h and 15h reaction times (For comparison, the reference profile V_2O_5 is also provided in the figure). As one can see, in the 15 min ball milled sample, the peaks from MgH_2 and V_2O_5 can be observed but no peaks from any form of reduced V or oxidized Mg can be confirmed. On the other hand, in the case of 1h ball milled sample, the relative intensity for both MgH_2 and V_2O_5 has decreased significantly whereas a new MgO peak can be observed. This peak can be confirmed again with higher relative peak intensity after 2h of mechanical milling. It is therefore clear from this observation that MgH_2 and V_2O_5 interact upon milling and leads to the oxidation of Mg. However, a notable point is that no XRD discernible phases of vanadium in any reduced form can be confirmed. Upon increasing the milling time further to 5h, the existence of a substantial quantity of MgO can be witnessed and only traces of MgH_2 and V_2O_5 remain in the powder. With further milling, i.e., between 10 and 15h, a complete transformation occurs and only monophase MgO with traces of Fe impurity can be observed. The absence of XRD peaks for such a large quantity of vanadium is possible only when reduced vanadium is in an amorphous state or it exists as a substituted dopant in the lattice of MgO. However, an extensive high resolution transmission electron microscopy study combined with EDS study clarifies that there are no amorphous regions in the sample and only a monophase with rock salt lattice can be confirmed (discussed in the proceeding section). This result validates the second possibility that after the chemical reduction, vanadium gets substituted in the MgO lattice, and it can be typified by a chemical formula $Mg_xV_yO_{x+y}$. It is interesting to note that this transformation is similar to the transformation we noticed in the Nb_2O_5/TiO_2 added MgH_2 reported by us, and we encourage the reader to refer these references [24–27].

The transformation of the additive demonstrated in Fig. 2 is under conditions where V_2O_5 exists in MgH_2 rich chemical proximity. On the other hand, to understand what happens when V_2O_5 exists in an MgH_2 deficient chemical proximity, another test sample, 0.25MgH_2+V_2O_5 was ball milled under identical conditions as that tested for the previous sample (i.e., MgH_2+0.25V_2O_5, Fig. 2). The observed XRDs of the sample, 0.25MgH_2+V_2O_5, mechanochemically reacted for 15 min, 1h, 2h, 5h, 10h and 15h are demonstrated in Fig. 3. As one can see, between 15 min and 1h milling, although the relative intensity of both MgH_2 and V_2O_5 has decreased, no clear evidence is found regarding the formation of any reduced species in these samples. However, upon increasing the milling time further to 2h, 5h, 10h and 15h, a new set of peaks is observed with the disappearance of all MgH_2 and V_2O_5 peaks. With careful observation we note that the new set of peaks are VO_2 with a small quantity of MgO also present. This suggests that when V_2O_5 is in an MgH_2 deficient environment, its partial reduction only to VO_2 happens. Conversely, when a sufficiently high quantity of MgH_2 exists further reduction can occur to assist the incorporation of V as the dopant species in the MgO lattice. It may also be noted that when we perform hydrogen storage experiments, we restrict the quantity of additives, typically to a maximum of 5 wt%. Since such a small quantity can exist only under MgH_2 rich environment, it is understandable that MgH_2+0.25V_2O_5, as explored in Fig. 2, provides the actual picture regarding the catalytic interaction between MgH_2 and the additive V_2O_5. This situation is also applicable to the previously reported Nb_2O_5/TiO_2 incorporated MgH_2 system which explored the formation of metal dissolved rock salt phases, $Mg_xNb_yO_{x+y}$/$Mg_xTi_yO_{x+y}$ [24–27]. One noted difference between these studies is that, under MgH_2 deficient environment whereas V_2O_5 transformed to VO_2, the additives Nb_2O_5 and TiO_2, respectively, transformed to NbO_2 and Ti_2O_3.

We further analyze the samples A1 and A2 by transmission electron

Table 1
Crystallographic details correspond to the observed rock salt phase in sample A2. Data corresponding to MgO is provided for reference.

sample	Observed phases	Structural Information				Crystallite size	Strain %
		Crystal struture	Space group	Lattice parameters	Cell volume		
A2	Oxidized Mg	Cubic	225:Fm-3m	a = b = c = 4.2146 Å	74.863 Å^3	6.2 nm	0.67 %
	Fe impurity	Cubic	229: Im-3m	a = b = c = 2.8734 Å	23.723 Å^3	–	0.50 %
MgO	MgO	Cubic	225:Fm-3m	a = b = c = 4.2186 Å	75.074 Å^3	11.6 nm	0.26 %

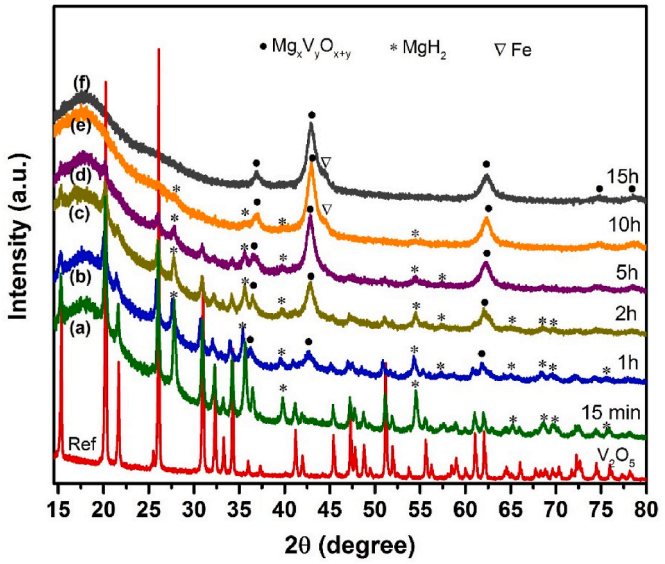

Fig. 2. XRD patterns correspond to MgH_2+0.25V_2O_5 reacted for (a) 15 min, (b) 1h, (c) 2h, (d) 5h, (e) 10h and (f) 15h. V_2O_5 is also included (profile in red) for comparison. (For interpretation of the references to colour in this figure legend, the reader is referred to the Web version of this article.)

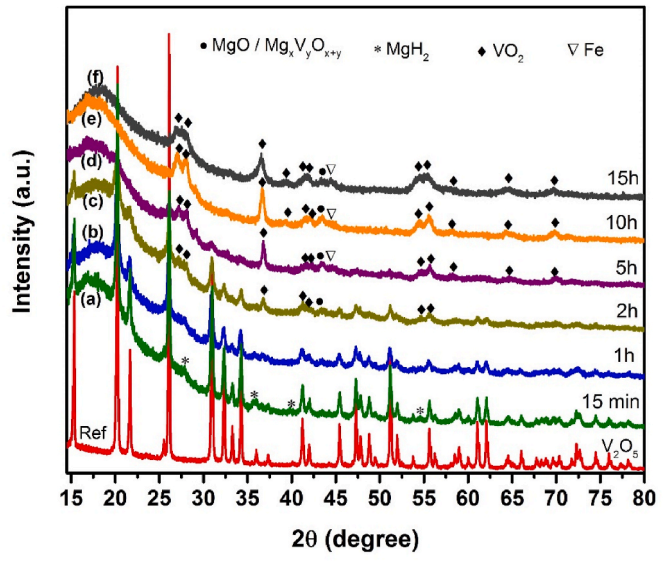

Fig. 3. XRD patterns correspond to 0.25MgH_2+V_2O_5 reacted for (a) 15 min, (b) 1h, (c) 2h, (d) 5h, (e) 10h and (f) 15h. V_2O_5 is also included (profile in red) for comparison. (For interpretation of the references to colour in this figure legend, the reader is referred to the Web version of this article.)

microscopy and scanning transmission electron microscopy. In Fig. 4, images "a", "b" and "c" showcase information regarding the particles existing in the V_2O_5 sample used in the current study. The image "a" suggests that the distribution of particles is roughly over 50–300 nm. For clarity, an individual particle is provided in image "b" and it reveals the smooth surface features of the V_2O_5 particles. A high-resolution image observed from a small segment of this particle is provided in the image "c". As seen, the crystallites contain no observable defects, and it can be further understood from the inset provided in image "c" (the inset corresponding to the highlighted portion in the same image). In this inset one can see the cleanly stacked array of atoms in the V_2O_5 lattice. The distribution of particles in sample A2 (images "d" and "e"), unlike in sample A1, is highly agglomerated, but it is possible to identify the existence of very small particles (roughly of size <5 nm, image "e"). An selected area electron diffraction (SAED) obtained from these particles is highlighted in image "f" and the corresponding hkl values of the ring patterns are provided in the figure. It is understood from the SAED that the sample contains only one rock salt phase, with lattice parameters a = b = c = 4.216 Å. Interestingly, we have also found no amorphous phase, which strengthens the view that the end product is V – dissolved MgO rock salt (conveniently referred as $Mg_xV_yO_{x+y}$). The transmission electron microscopy images recorded for sample A2 in three different magnifications are provided in images "g", "h" and "i". The images "g" and "h" suggest that the typical size of any individual particle can be between 2 and 5 nm but these particles are heavily agglomerated. This can be further understood with the high resolution image "i" shown in Fig. 4. Unlike the lattice of V_2O_5 shown in image "c", in sample A2, the lattice is substantially defective, which can be understood from the inset provided in "i". Closer to the defective region in image "i", the identified fringe spacing 0.24 nm (the plane is marked by parallel yellow lines) correspond to that of $d_{(111)}$ from the rock salt lattice, MgO/$Mg_xV_yO_{x+y}$. The value obtained from SAED (0.24 nm) and XRD (0.243 nm) are in agreement with the fringe spacing noted from the image "i" in Fig. 4.

We have also analyzed the distribution of elements in sample A2 through high-angle annular dark-field scanning transmission electron microscopy (HAADF-STEM), which is a Z contrast imaging technique. A HAADF-STEM image observed for the particle subjected for this analysis is provided in image "a", Fig. 5. From the distinct image contrast observed in this image, especially from the directional extension of bright spots, it can be inferred that the distribution of the heavier element among V, Mg and O may be richer in some spots over the others. It can be further understood by comparing the elemental distribution maps provided for Mg–V–O and Mg–V (images, "b" and "c"), that these regions contain more vanadium than in the bulk regions. From the individual elemental distribution maps provided for V, Mg and O in images, "d", "e" and "f", it is clear that, regardless of distribution difference between Mg and V, oxygen is found everywhere, suggesting that both V and Mg exist in the oxygen locality. It gives us an understanding that although A2 may be predominantly V dissolved MgO (typified by $Mg_xV_yO_{x+y}$), V enriched spots indeed exist in the interface of these particles. It is also possible that the concentration of V is different in the surface and bulk of individual $Mg_xV_yO_{x+y}$ particles, as observed in one of our recent works [29].

Further on, in order to obtain more information regarding the chemical state of V, Mg and O, the sample A2 is studied by X ray photoelectron spectroscopy. In Fig. 6, the XPS high resolution scan profiles for (a) O1s and V2p, (b) Mg2p peaks are provided with the deconvoluted peaks of the corresponding complex spectra (note: the deconvolution of V2p region in the current case is complex due to the low relative peak intensity and the possible existence of satellite peaks. Therefore, to avoid the erroneous indexing of peaks, instead of

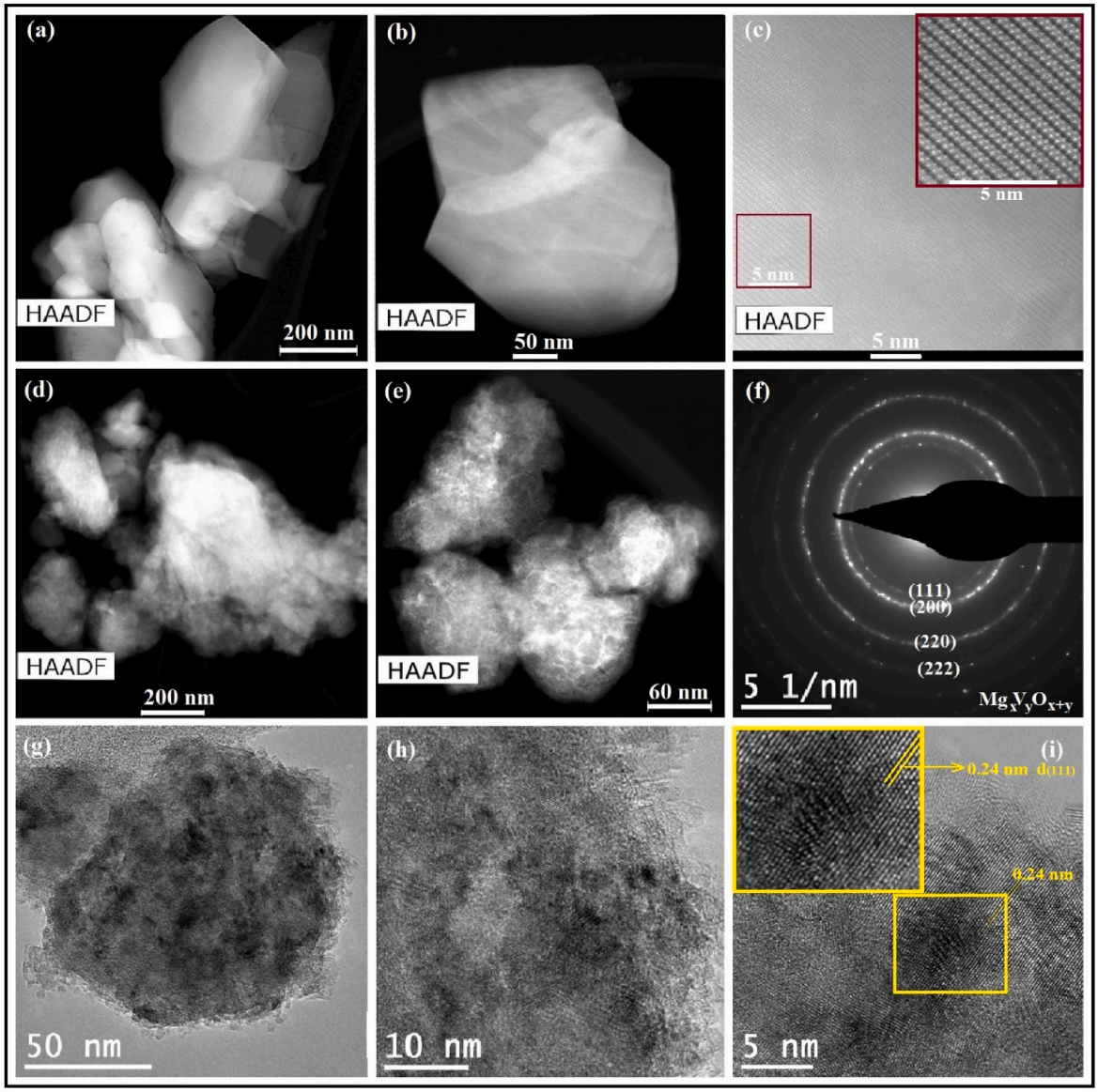

Fig. 4. (a), (b) and (c), HAADF-STEM images of V_2O_5 (A1) obtained at different magnifications, (d) and (e) HAADF-STEM images of 15h reacted MgH_2+0.25V_2O_5 (A2), (f) SAED observed for the 15h reacted MgH_2+0.25V_2O_5, (g), (h) and (i) HRTEM images of A2 obtained at different magnifications.

deconvolution we have marked the corresponding BE of all V2p states in the figure. For a detailed overview of de-convoluted V2p XPS spectra for a standard case, the reader is suggested to follow the works of Silversmit et al. and Rakshit et al. [43–45]). From the marked BE values corresponding to different oxidation states of vanadium (Fig. 6a), it can be understood that in sample A2, V exists in a mixed valence state. The presence of V(IV) can be attributed to the VO_2 traces existing at the surface of $Mg_xV_yO_{x+y}$ rock salt particles, whereas V(II) and V(III) can be due to the substitution of V in the rock salt structure. Previous works on metals doped rock salt structures, e.g, MgO and CaO reveals that metal cations with 3+ valence state can exist in the rock salt lattice through the incorporation of charge compensating cationic/anionic vacancies [46, 47]. Although the XRD and TEM investigations do not reveal the presence of metallic V in the powder, as per the XPS observation, the presence of V(0) traces cannot be ruled out in sample A2. The O1s region exhibits three contributions with peak signals at the BE values 531.3 eV, 529.3 eV and 527 eV. In the literature, oxygen signals from MgO and VO_x are found at 531.1 eV and 530.0 eV [43,48]. From these inputs, for the current case we attribute the O1s peak from the higher BE side with the Mg rich $Mg_xV_yO_{x+y}$ and the peak at the lower BE side with the V rich part of $Mg_xV_yO_{x+y}$ rock salt. It is reasonable to draw this conclusion as EDS elemental chemical maps provide evidence for the existence of such species in sample A2. Another minor contribution from yet another oxygen bearing phase in A2 can be understood from a low intensity peak at 527 eV. O1s XPS peak at BE closer to this value is reported for a few systems [49,50] and this signal was attributed to the oxygen existence under a highly cationic chemical environment [49]. With this input, we believe that the peak observed at 527 eV in the current case may be due to the presence of highly oxygen deficient VO_x or $Mg_xV_yO_{x+y}$ species in sample A2. The deconvoluted Mg1s profile as given in Fig. 6b also shows two contributions, one at BE, 50.5 eV and the other at 48.9 eV. Both peaks can be attributed to oxidized Mg [51]; for instance, one due to the Mg rich $Mg_xV_yO_{x+y}$ and the other is due to V rich $Mg_xV_yO_{x+y}$ rock salt phase in A2. This assertion is in agreement with the O1s peak profiles shown in Fig. 6a.

After the above sample tests, our interest is to test what influence does the end rock salt A2 (i.e. $Mg_xV_yO_{x+y}$) make to MgH_2 when existing as an additive along with MgH_2. If the oxidized Mg existing in A2 is a pure MgO rock salt phase, its incorporation with MgH_2 is expected to provide a detrimental effect because MgO is known as a surface

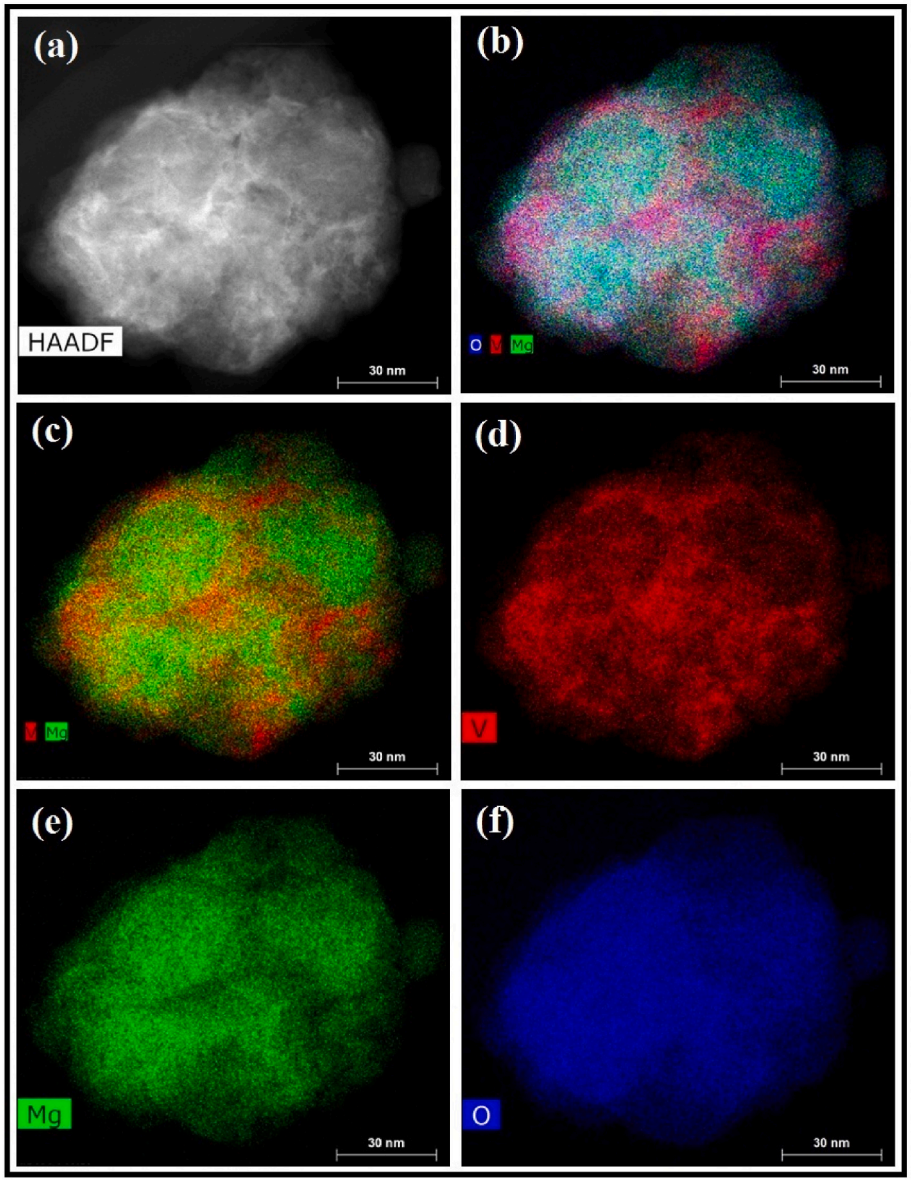

Fig. 5. EDS elemental chemical distribution map corresponding to the sample A2. Image sequence: (a) HAADF of the selected particle, (b) scan map for elements Mg, V and O together, (c) Mg and V together, (d) V alone, (e) Mg alone and (f) O alone.

passivator for the MgH_2 system. In this context, we have incorporated a 5 wt% of A2 with MgH_2 and performed a differential scanning calorimetry (DSC) study. For comparison a 5 wt% of A1 added MgH_2 and clean MgH_2 were also tested under identical conditions and the observed profiles are provided in Fig. 7. As one can see, in the as-synthesized pure MgH_2 sample, peak endothermic dehydrogenation occurs at 375 °C. Incorporation of a 5 wt% A1 (i.e. V_2O_5), lowers the dehydrogenation temperature of MgH_2 by 50 °C. Interestingly, the additive A2 also decreased the dehydrogenation temperature almost with similar effect and in fact we observed a slightly better effect. The peak endothermic dehydrogenation temperature in the case of A2 added MgH_2 is roughly 2 °C lower than the case of A1 and also the onset dehydrogenation temperature is roughly 20 °C smaller for A2 with respect to A1. It suggests that a catalytic behavioral change happens to MgO when metal atoms get substituted in the MgO lattice. The dehydrogenation enthalpy change (ΔH) was also extracted from the DSC profiles, and it was found to be 74.2 kJ/mol for the A1 added sample and 74.5 kJ/mol for the A2 added sample. These values are comparable with the previous reports [25,28]. After the DSC study, we also test the dehydrogenation/rehydrogenation kinetics of A1 and A2 added MgH_2 and the results are provided in Fig. 8. As one can see, the V_2O_5 added MgH_2 sample at the dehydrogenation temperature of 300 °C (1 bar) releases 6 wt% hydrogen within 6h (21600 s) and the other sample (A2 added MgH_2) also provides nearly identical kinetic performance. When rehydrogenated at 300 °C/5 bar hydrogen pressure both the samples restore over 95% of the desorbed hydrogen within 15 min (900 s). The hydrogen storage test results provided in Figs. 7 and 8, are informative to highlight that V dissolved MgO is catalytically more active than clean MgO.

After the kinetics studies, we have analyzed the A1 and A2 added MgH_2 powder samples by XRD technique. In Fig. 9, the provided sequence of XRD profiles is as in the following, (a) 5 wt% A1 added MgH_2 sample in the as-prepared state, (b) 5 wt% A1 added sample after dehydrogenation treatment, (c) after re-hydrogenating the above dehydrogenated sample, (d) 5 wt% A2 added MgH_2 sample in the as-prepared state, (e) 5 wt% A2 added sample after dehydrogenation treatment and (f) after re-hydrogenating the dehydrogenated sample (i.e., A2 added sample). These XRDs show the presence of Mg in the

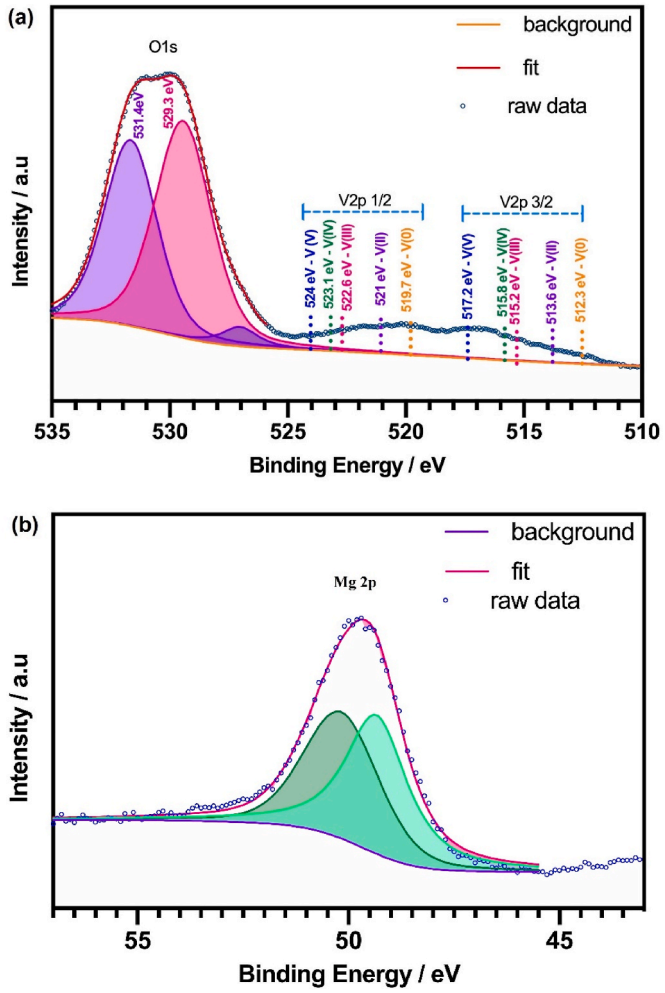

Fig. 6. XPS spectra corresponding to (a) O1s and V2p, (b) Mg2p for the sample A2 (i.e. 15h reacted MgH_2+0.25V_2O_5).

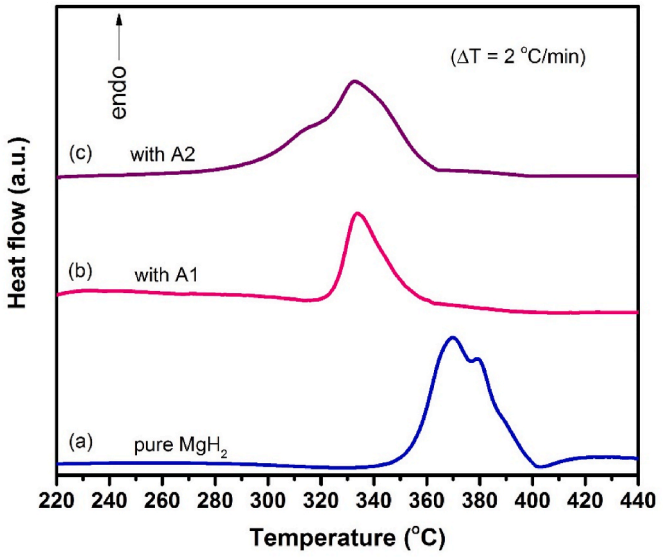

Fig. 7. DSC profiles corresponding to (a) clean MgH_2 without any additives (i.e. as-synthesized MgH_2), (b) MgH_2 with 5 wt% A1 as additive, and (c) MgH_2 with 5 wt% A2 as additive.

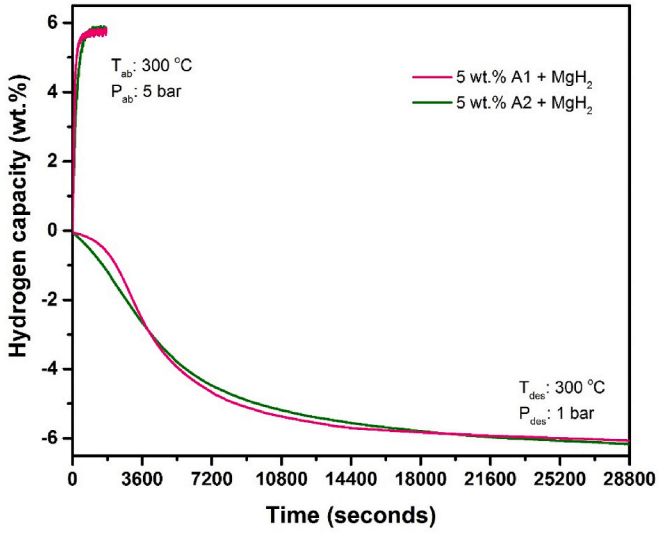

Fig. 8. Dehydrogenation and subsequent re-hydrogenation kinetic profiles correspond to MgH_2 with 5 wt% A1 and A2 as additives for MgH_2.

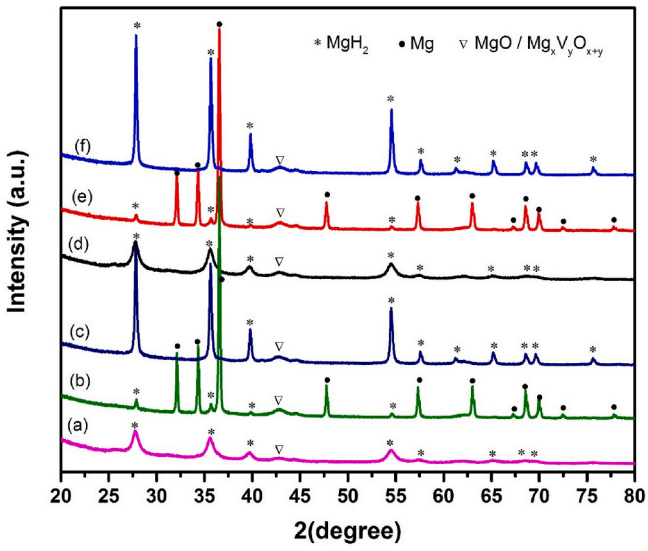

Fig. 9. XRD patterns corresponding to, (a) the as-prepared 5 wt% A1 added MgH_2 sample, (b) the 5 wt% A1 added MgH_2 sample after dehydrogenation at 300 °C (1 bar), (c) the 5 wt% A1 added MgH_2 sample after hydrogen uptake at 5 bar/300 °C (d) the as-prepared 5 wt% A2 added MgH_2 sample, (e) the 5 wt% A2 added MgH_2 sample after dehydrogenation treatment at 300 °C (1 bar) and, (f) the 5 wt% A2 added MgH_2 sample after re-hydrogenation at 5 bar/300 °C.

dehydrogenated sample and its reverse conversion to the hydride phase under the reaction conditions employed for the kinetic measurements discussed in Fig. 8. Moreover, in all these XRDs, no direct evidence for the V based compounds can be observed, except that the MgO based rock salt phase can be noted at the 2θ position ~42.7°. The vanadium is expected to be dissolved in MgO, as explored in detail in the aforementioned sections (refer information based on Figs.1–7). We have also calculated the crystallite size from the XRD profiles for all the samples and it provides information regarding the phase/microstructure evolution in different stages of the reaction. We have observed that in both the cases of A1 and A2, the microstructural evolution of the observed phases is closely similar to each other. For instance, the calculated crystallite size from profiles (a), (b) and (c) respectively, 10.2 nm, 39.3 nm and 35.2 nm. The observed crystallite size values from (d), (e) and (f) respectively, 10.6 nm, 38.2 nm and 39 nm. This trend is in agreement

with our earlier report [52], whereas it is also clear that the observed improved hydrogen storage performance is mainly due to the catalytic activity, though the observed small size is an added advantage for both the samples.

In summary, it can be said that in a MgH_2 system when we add a small amount of V_2O_5 as an additive, the additive chemically interacts with MgH_2 and makes a rock salt product, typified by $Mg_xV_yO_{x+y}$. Interestingly, the total dissolution of V in MgO makes a behavioral change to MgO. For instance, MgO rock salt is an inert hydrogen impermeable layer in the MgH_2 system, and its existence is usually undesired as it passivates the surface of MgH_2. However, metal (in the current case, it is V) dissolution changes the entire chemical behavior of MgO, as the V dissolved MgO is found to be quite active as a catalyst for MgH_2. Behavioral transformations like these are very interesting and exploring such details provides significant impact on the understanding of how catalysts work under different circumstances. It is quite interesting to note that our previous studies on Nb_2O_5 and TiO_2 additives also revealed the formation of metals dissolved rock salt in MgH_2 system [24–27] and, likewise improved hydrogen storage performance. More oxides need to be tested in the future to provide clues for formulating a generalized catalytic mechanism for metal oxides incorporated MgH_2 for hydrogen storage applications.

4. Conclusions

In the current study, we have systematically studied the interaction between MgH_2 and the V_2O_5 additive and reached the following conclusions.

1. MgH_2 and V_2O_5 interact chemically upon mechanical milling. Under MgH_2 rich environment, the interaction leads to the formation of a mono-phase rock salt oxide, typified by $Mg_xV_yO_{x+y}$.
2. Under MgH_2 deficient environment partial reduction of V_2O_5 ends up with the formation of another stable oxide VO_2.
3. Dissolution of V in the MgO rock salt may be different in the bulk and the surface, as V rich spots are identified at the grain boundaries.
4. The V dissolution in MgO alters the behavior of MgO from being catalytically passive to catalytically active for the MgH_2 system. The DSC and the hydrogen storage tests performed in the current study provide convincing evidence that V dissolved MgO presents a totally modified catalytic behavior for MgH_2.

Declaration of competing interest

The authors declare that they have no known competing financial interests or personal relationships that could have appeared to influence the work reported in this paper.

Acknowledgement

This article was supported by the projects UIDB/00481/2020 and UIDP/00481/2020 - Fundação para a Ciência e a Tecnologia, DOI 10.54499/UIDB/00481/2020 (https://doi.org/10.54499/UIDB/00481/2020) and DOI 10.54499/UIDP/00481/2020 (https://doi.org/10.54499/UIDP/00481/2020). The work is also supported by CENTRO-01-0145-FEDER-022083 - Centro Portugal Regional Operational Programme (Centro 2020), under the PORTUGAL 2020 Partnership Agreement, through the European Regional Development Fund (ERDF). D. P acknowledges FCT, Portugal for the financial support with reference CEECIND/04158/2017 (https://doi.org/10.54499/CEECIND/04158/2017/CP1459/CT0029).This project has also received funding from the SMART-ER project, funded by the European Union's Horizon 2020 research and innovation programme under Grant Agreement #101016888. The authors are also grateful for the financial support granted by the Recovery and Resilience Plan (PRR) and by the Next Generation EU European Funds to Universidade de Aveiro, through the Agenda for Business Innovation "NGS - Next Generation Storage" (Project no 02/C05-i01.01/2022 with the application C644936001-00000045).

References

[1] Pukazhselvan D, Sandhya KS, Fagg DP. 5 - Nanostructured advanced materials for hydrogen storage. In: Naushad M, Saravanan R, Raju K, editors. Nanomaterials for Sustainable energy and environmental Remediation. Elsevier; 2020. p. 97–163.
[2] Ghorbani B, Zendehboudi S, Saady NMC, Dusseault MB. Hydrogen storage in North America: status, prospects, and challenges. J Environ Chem Eng 2023;11:109957.
[3] D P, Çaha I, Loureiro FJA, Shaula AL, Mikhalev SM, Deepak FL, et al. Superior catalytic effect of titania - porous carbon composite for the storage of hydrogen in MgH_2 and lithium in a Li ion battery. Int J Hydrogen Energy 2023;48:23917–29.
[4] Hou Q, Yang X, Zhang J. Review on hydrogen storage performance of MgH_2: development and trends. ChemistrySelect 2021;6:1589–606.
[5] Xu N, Wang K, Zhu Y, Zhang Y. PdNi biatomic clusters from metallene unlock record-low onset dehydrogenation temperature for bulk-MgH_2. Adv Mater 2023;35:2303173.
[6] Hou Q, Zhang J, Zheng ZA, Yang X, Ding Z. Ni_3Fe/BC nanocatalysts based on biomass charcoal self-reduction achieves excellent hydrogen storage performance of MgH_2. Dalton Trans 2022;51:14960–9.
[7] Wang S, Gao M, Yao Z, Xian K, Wu M, Liu Y, et al. High-loading, ultrafine Ni nanoparticles dispersed on porous hollow carbon nanospheres for fast (de) hydrogenation kinetics of MgH_2. J Magnesium Alloys 2022;10:3354–66.
[8] Zhang XL, Liu YF, Zhang X, Hu JJ, Gao MX, Pan HG. Empowering hydrogen storage performance of MgH_2 by nanoengineering and nanocatalysis. Mater. Today Nano 2020;9:100064.
[9] Yu Z, Liu X, Liu Y, Li Y, Zhang Z, Chen K, et al. Synergetic catalysis of Ni@C@CeO2 for driving ab/desorption of MgH_2 at moderate temperature. Fuel 2024;357:129726.
[10] Ma Z, Ni J, Qian Z, Liu J, Zhu Y, Zhang J, et al. Short-range nanoreaction effect on the hydrogen desorption behaviors of the MgH_2–Ni@C composite. ACS Appl Mater Interfaces 2023;15:1384–91.
[11] Maurizio C, Checchetto R, Trapananti A, Rizzo A, D'Acapito F, Miotello A. In situ X-ray absorption spectroscopy–X-ray diffraction investigation of Nb–H nanoclusters in MgH_2 during hydrogen desorption. J Phys Chem C 2015;119:7765–70.
[12] Pukazhselvan D, Sandhya KS, Ramasamy D, Shaula A, Fagg DP. Transformation of metallic Ti to TiH_2 phase in the Ti/MgH_2 composite and its influence on the hydrogen storage behavior of MgH_2. ChemPhysChem 2020;21:1195–201.
[13] Barkhordarian G, Klassen T, Bormann R. Catalytic mechanism of transition-metal compounds on Mg hydrogen sorption reaction. J Phys Chem B 2006;110:11020–4.
[14] Pukazhselvan D, Çaha I, Mikhalev S, Deepak FL, Fagg DP. A highly active additive for magnesium hydride from the MgO–TiO_2 mixed oxide family: magnesium dititanate. Int J Hydrogen Energy 2023.
[15] Bhat VV, Rougier A, Aymard L, Darok X, Nazri G, Tarascon JM. Catalytic activity of oxides and halides on hydrogen storage of MgH_2. J Power Sources 2006;159:107–10.
[16] Korablov D, Nielsen TK, Besenbacher F, Jensen TR. Mechanism and kinetics of early transition metal hydrides, oxides, and chlorides to enhance hydrogen release and uptake properties of MgH_2. Powder Diffr 2015;30:S9–15.
[17] Liang G, Huot J, Boily S, Van Neste A, Schulz R. Catalytic effect of transition metals on hydrogen sorption in nanocrystalline ball milled MgH_2–Tm (Tm=Ti, V, Mn, Fe and Ni) systems. J Alloys Compd 1999;292:247–52.
[18] Malka IE, Pisarek M, Czujko T, Bystrzycki J. A study of the ZrF_4, NbF_5, TaF_5, and $TiCl_3$ influences on the MgH_2 sorption properties. Int J Hydrogen Energy 2011;36:12909–17.
[19] Ren C, Fang ZZ, Zhou C, Lu J, Ren Y, Zhang X. Hydrogen storage properties of magnesium hydride with V-based additives. J Phys Chem C 2014;118:21778–84.
[20] Wang Y, Zhang Q, Wang Y, Jiao L, Yuan H. Catalytic effects of different Ti-based materials on dehydrogenation performances of MgH_2. J Alloys Compd 2015;645:S509–12.
[21] Friedrichs O, Aguey-Zinsou F, Fernández JRA, Sánchez-López JC, Justo A, Klassen T, et al. MgH_2 with Nb_2O_5 as additive, for hydrogen storage: chemical, structural and kinetic behavior with heating. Acta Mater 2006;54:105–10.
[22] Friedrichs O, Martínez-Martínez D, Guilera G, Sánchez López JC, Fernández A. In situ energy-dispersive XAS and XRD study of the superior hydrogen storage system MgH_2/Nb_2O_5. J Phys Chem C 2007;111:10700–6.
[23] Nielsen TK, Jensen TR. MgH_2–Nb_2O_5 investigated by in situ synchrotron X-ray diffraction. Int J Hydrogen Energy 2012;37:13409–16.
[24] Pukazhselvan D, Nasani N, Sandhya KS, Singh B, Bdikin I, Koga N, et al. Role of chemical interaction between MgH_2 and TiO_2 additive on the hydrogen storage behavior of MgH_2. Appl Surf Sci 2017;420:740–5.
[25] Pukazhselvan D, Nasani N, Correia P, Carbó-Argibay E, Otero-Irurueta G, Stroppa DG, et al. Evolution of reduced Ti containing phase(s) in MgH_2/TiO_2 system and its effect on the hydrogen storage behavior of MgH2. J Power Sources 2017;362:174–83.
[26] Pukazhselvan D, Bdikin I, Perez J, Carbó-Argibay E, Antunes I, Stroppa DG, et al. Formation of Mg–Nb–O rock salt structures in a series of mechanochemically activated MgH_2 + nNb_2O_5 (n = 0.083–1.50) mixtures. Int J Hydrogen Energy 2016;41:2677–88.
[27] Pukazhselvan D, Perez J, Nasani N, Bdikin I, Kovalevsky AV, Fagg DP. Formation of $Mg_xNb_yO_{x+y}$ through the mechanochemical reaction of MgH_2 and Nb_2O_5, and its

effect on the hydrogen-storage behavior of MgH2. ChemPhysChem 2016;17:178–83.
[28] Pukazhselvan D, Sandhya KS, Nasani N, Paul Fagg D. Chemical transformation of additive phase in MgH_2/CeO_2 hydrogen storage system and its effect on catalytic performance. Appl Surf Sci 2021;561:150062.
[29] Pukazhselvan D, Çaha I, Jakka SK, Graça VCD, Holz LIV, Soares MJ, et al. Catalysis of ceria incorporated magnesium hydride: a follow up study. Int J Hydrogen Energy 2022;47:28978–92.
[30] Pukazhselvan D, Reis Silva DA, Sandhya KS, Fateixa S, Shaula A, Nogueira H, et al. Interaction of zirconia with magnesium hydride and its influence on the hydrogen storage behavior of magnesium hydride. Int J Hydrogen Energy 2022;47:21760–71.
[31] Pukazhselvan D, Sandhya KS, Ramasamy D, Shaula A, Bdikin I, Fagg DP. Active catalytic species generated in situ in zirconia incorporated hydrogen storage material magnesium hydride. J Magnesium Alloys 2022;10:786–96.
[32] Pukazhselvan D, Nasani N, Yang T, Ramasamy D, Shaula A, Fagg DP. Chemically transformed additive phases in Mg_2TiO_4 and $MgTiO_3$ loaded hydrogen storage system MgH_2. Appl Surf Sci 2019;472:99–104.
[33] Min Dai GL, Zhang Zhao, Li Zhi, Cao Hujun, Chen Ping. Room temperature hydrogen absorption of V_2O_5 catalyzed MgH_2/Mg. Acta Chim Sin 2022;80:303–9.
[34] Wang Z, Ren Z, Jian N, Gao M, Hu J, Du F, et al. Vanadium oxide nanoparticles supported on cubic carbon nanoboxes as highly active catalyst precursors for hydrogen storage in MgH_2. J Mater Chem A 2018;6:16177–85.
[35] Oelerich W, Klassen T, Bormann R. Metal oxides as catalysts for improved hydrogen sorption in nanocrystalline Mg-based materials. J Alloys Compd 2001;315:237–42.
[36] Oelerich W, Klassen T, Bormann R. Comparison of the catalytic effects of V, V_2O_5, VN, and VC on the hydrogen sorption of nanocrystalline Mg. J Alloys Compd 2001;322:L5–9.
[37] Grigorova E, Khristov M, Peshev P, Nihtianova D, Velichkova N, Atanasova G. Hydrogen sorption properties of a MgH_2-V_2O_5 composite prepared by ball milling. Bulg Chem Commun 2013;45:280–7.
[38] Carrazán SRG, Peres C, Bernard JP, Ruwet M, Ruiz R, Delmon B. Catalytic synergy in the oxidative dehydrogenation of propane over MgVO catalysts. J Catal 1996;158:452–76.
[39] Carrazán SRG, Peres C, Ruwet M, Ruiz P, Delmon B. Solid state reaction in Mg-V-O-Sb catalysts. Solid State Ionics 1997;101–103:737–42.
[40] Jung KS, Lee EY, Lee KS. Catalytic effects of metal oxide on hydrogen absorption of magnesium metal hydride. J Alloys Compd 2006;421:179–84.
[41] Pukazhselvan D, Otero-Irurueta G, Pérez J, Singh B, Bdikin I, Singh MK, et al. Crystal structure, phase stoichiometry and chemical environment of $Mg_xNb_yO_{x+y}$ nanoparticles and their impact on hydrogen storage in MgH_2. Int J Hydrogen Energy 2016;41:11709–15.
[42] McCusker LB, Von Dreele RB, Cox DE, Louer D, Scardi P. Rietveld refinement guidelines. J Appl Crystallogr 1999;32:36–50.
[43] Silversmit G, Depla D, Poelman H, Marin GB, De Gryse R. Determination of the V2p XPS binding energies for different vanadium oxidation states (V^{5+} to V^{0+}). J Electron Spectrosc Relat Phenom 2004;135:167–75.
[44] Silversmit G, Depla D, Poelman H, Marin GB, De Gryse R. An XPS study on the surface reduction of V_2O_5(001) induced by Ar^+ ion bombardment. Surf Sci 2006;600:3512–7.
[45] Rakshit A, Mukherjee M, Chakraborty S. Effect of oxygen content on the electrical properties of sputter deposited vanadium oxide thin-films. Mater Sci Semicond Process 2018;88:127–31.
[46] Benedetti S, Nilius N, Valeri S. Chromium-doped MgO thin films: morphology, electronic structure, and segregation effects. J Phys Chem C 2015;119:25469–75.
[47] Stavale F, Shao X, Nilius N, Freund H-J, Prada S, Giordano L, et al. Donor characteristics of transition-metal-doped oxides: Cr-doped MgO versus Mo-doped CaO. J Am Chem Soc 2012;134:11380–3.
[48] Burke PJ, Bayindir Z, Kipouros GJ. X-Ray photoelectron spectroscopy (XPS) investigation of the surface film on magnesium powders. Appl Spectrosc 2012;66:510–8.
[49] Kulkarni GU, Laruelle S, Roberts MW. The oxygen state active in the catalytic oxidation of carbon monoxide at a caesium surface: isolation of the reactive anionic $CO2^{\delta-}$ species. Chem Commun 1996:9–10.
[50] Cao C, Abate II, Sivonxay E, Shyam B, Jia C, Moritz B, et al. Solid electrolyte interphase on native oxide-terminated silicon anodes for Li-ion batteries. Joule 2019;3:762–81.
[51] Ardizzone S, Bianchi CL, Fadoni M, Vercelli B. Magnesium salts and oxide: an XPS overview. Appl Surf Sci 1997;119:253–9.
[52] Pukazhselvan D, Capurso G, Maddalena A, Lo Russo S, Fagg DP. Hydrogen storage characteristics of magnesium impregnated on the porous channels of activated charcoal scaffold. Int J Hydrogen Energy 2014;39:20045–53.